

Received August 27, 2019, accepted September 16, 2019, date of publication October 1, 2019, date of current version October 15, 2019.

Digital Object Identifier 10.1109/ACCESS.2019.2944955

Reliability Prediction of Highly Scaled MOSFET Devices via Fractal Structure of Spatial Defects

SEONG-JOON KIM¹, MAN SOO KIM², AND SUK JOO BAE³

¹Department of Industrial Engineering, Chosun University, Gwangju 61452, South Korea

²ILS R&D Lab, LIG Nex1, Gyeonggi 13488, South Korea

³Department of Industrial Engineering, Hanyang University, Seoul 04763, South Korea

Corresponding author: Suk Joo Bae (sjbae@hanyang.ac.kr)

The work of S.-J. Kim was supported in part by the Basic Science Research Program through the National Research Foundation of Korea (NRF) funded by the Ministry of Education under Grant 2017R1D1A1B03032543. The work of S. J. Bae was supported in part by the Basic Science Research Program through the National Research Foundation of Korea (NRF) funded by the Ministry of Education under Grant 2018R1D1A1A09083149.

ABSTRACT The needs for continuous size reduction of metal-oxide-semiconductor field effect transistor (MOSFET) devices can cause serious reliability concerns. In particular, gate oxide breakdown is a key mechanism concerning the lifetimes of MOSFET devices. In this paper, several spatial point processes are employed to represent general patterns of defect generation in gate oxide. By defining oxide breakdown as a creation of conduction path connecting two oxide interfaces by overlapped defects, percolation models are discussed to predict reliability of MOSFET devices in terms of critical defect density. In the final, we proposed a method to evaluate lifetimes of area-scaled gate oxides in MOSFET devices mainly through their fractal structure. The method suggests an easy way to predict the lifetimes of the devices with area-scaled gate oxides by examining their fractal structure through a fractal dimension without involving breakdown distributions of gate oxides with different areas.


INDEX TERMS Fractal structure, oxide breakdown, percolation model, spatial point process, time-dependent dielectric breakdown.

I. INTRODUCTION

A metal-oxide-semiconductor field effect transistor (MOSFET) device operates at lower electric field. The oxide layer slowly degrades as lower electric field is applied during operating time. This phenomenon (called “time dependent dielectric breakdown” (TDDB)) is one of key limitations to reliability of MOSFET devices. The oxide breakdown of MOSFET device can be largely classified into two types: intrinsic and extrinsic breakdown. the intrinsic breakdown, sometimes referred to as “wear-out”, is intrinsic to materials consisting of the gate oxide. On the contrary, the extrinsic breakdown is generally caused by defects generated in a series of manufacturing processes such as metallic, organic, or other contaminants on the crystalline silicon surface. With the trend of continuous reduction of oxide thickness and increase of electric field, the intrinsic breakdown has become the most likely problem as far as oxide reliability is concerned. Peng and Feng [1] characterized the overall

intrinsic breakdown process of ultrathin gate oxides as a logistic degradation process with a random onset time.

Intrinsic breakdown generally begins with defect (or trap) generation and resulting formation of bulk oxide states as the device is stressed at elevated voltage and temperature [2]. With increasing defects during electrical stressing, conducting path of neighboring defects can be generated from the top to the bottom of the oxide layer, resulting in the dielectric breakdown. This is called “percolation” because electrons can percolate through the oxide layer along this conductive path [3]. The schematic illustration of a percolation path built by sphere-shaped defects is given in Figure 1. The percolation path depends highly on the patterns of defect generation, *i.e.*, whether the defects are generated randomly or in cluster. It has been generally accepted that defects increase in the oxide layer as the current is injected over time, then a breakdown is triggered whenever the defects reach at the critical level of defect density [4], [5]. To accurately predict reliability of the MOSFET device, especially of newly developed devices with gate oxide as thin as 1 nm, well-defined models for defect generation and understanding of

The associate editor coordinating the review of this manuscript and approving it for publication was Zhaojun Li .

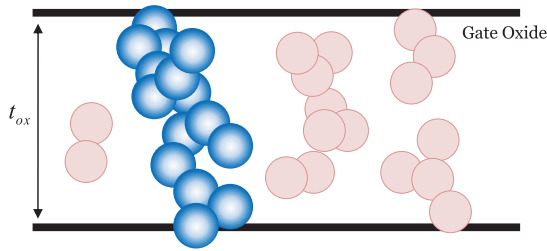


FIGURE 1. A schematic illustration of a percolation model (The percolation path is indicated by heavily shaded spheres. t_{ox} denotes oxide thickness).

their physical structure must be established *a priori*. Nevertheless, the procedure for determining correct distribution of defect density and proper way to formulate defect effects on oxide lifetime have not been completely resolved yet.

This paper proposes a new method to evaluate lifetimes of area-scaled gate oxide in the operation of MOSFET devices, mainly based on a percolation model for spatially distributed defects and its fractal structure. Several spatial point processes are introduced to model the patterns of defect generation, and the oxide lifetime is estimated by calculating critical defect density forming the percolation path by spatial defects. Many existing studies on the reliability of MOSFET devices have been focused on physical aspects of the percolation models. Furthermore, the percolation models have been simply constructed on the basis of randomly generated defect structure. Recently, Yuan and Zhu [6] proposed a spatio-temporal percolation model considering the relationship between defect occurrences and oxide failure-times. Their percolation model was constructed based on the random generating structure of sphere-shaped defects using a homogeneous Poisson process. Later, Kim et al. [7] proposes a spatio-temporal percolation model for progressive breakdowns of ultra-thin gate oxide in a convolution form. Because spatial defect patterns in the oxide layer connote its own physical mechanisms for defect generation, spatial defect distribution must be explicitly expressed for reliability analysis of MOSFET devices. Nevertheless, relatively less efforts have been devoted to evaluation of oxide reliability by taking spatially distributed defects in the oxide into account.

II. SPATIAL MODELING OF DEFECT GENERATION

Degraeve et al. [4] assumed that electron defects are generated randomly in the oxide layer with constant defect generation probability p . The only parameter in this model is an effective radius of the electron defect, r . The random defect generation procedure can be simply modeled by a (*spatial*) *homogeneous Poisson process* (HPP). The detailed explanation of spatial HPP is given in Appendix A. The random defect generation procedure by Degraeve et al. [4] is realized by placing spheres with common radius r on the points following the homogeneous Poisson point process.

Khosru et al. [8] introduced an exponentially decreasing function from the oxide interface to a spatial distribution of hole traps in the oxide layer. Its probability function of trap

generation is

$$p(s) = k_0 e^{-s/\eta}, \quad (1)$$

where s is the distance from the interface, k_0 is a constant, and η represents a decay length from the interface. The model (1) is called “gradient percolation” which is one of inhomogeneous percolation models introduced by Rosso et al. [9]. Such inhomogeneous defects pattern can be modeled by a (*spatial*) *nonhomogeneous Poisson process* (NHPP). The details on the NHPP is given in Appendix B. Quintanilla and Torquato [10] proposed an intensity function for spheres following the NHPP as

$$\lambda(x, y) = \frac{C_0}{r^2} e^{-\kappa y/L}, \quad (2)$$

where C_0 is a constant, L is the length scale of the entire system, and κ is the length scale of the variation of $\lambda(x, y)$ for Cartesian coordinates $\mathbf{x} = (x, y)$. The exponentially decreasing pattern of defects from the interface can be specified by the NHPP with the intensity function (2).

In general, defects are more likely to be formed around the neighborhood of other defects. Chandra et al. [11] observed that defects occur mainly within an “interacting distance”, which is defined as the minimum distance between two defects of the same kind that do not interact. Uno et al. [12] defined the defect generation probability p as a function of the distance from other existing defects:

$$p = \begin{cases} c\zeta & \text{Within } 2r \text{ from existing traps} \\ \zeta & \text{Otherwise} \end{cases} \quad (3)$$

where c is a constant larger than unity to represent the fact that new defects are more likely to occur around other defects and ζ is a constant determined by a normalization integral. To generalize the Eq. (3) in a more flexible framework, we apply a *pair-potential Markov point process* [13] to the defects distributed in the oxide layer. The pair-potential Markov point process have been most commonly used to model a repulsive interaction between points. This more highly developed point process has the potential in generalizing the defect patterns formed in the oxide, including the defects’ attraction/repulsion toward each other (see Appendix C for details on pair-potential Markov point process).

III. PERCOLATION MODELS FOR OXIDE BREAKDOWN

Several percolation models have been applied to describe the oxide breakdown and successfully explained theoretical and experimental results of the oxide breakdown. We will introduce three important percolation models in turn.

A. TILE-BASED PERCOLATION MODEL

Suñé et al. [14] assumed that the breakdown of oxide layer is final consequence of degradation of the oxide layer. The obtained distribution of failures preserves main properties of extreme-value statistics. The main idea is as follows. Suppose that the total area of gate oxide S_T is divided up into

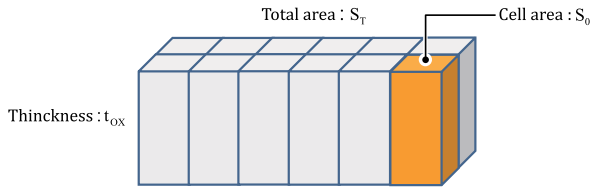


FIGURE 2. Suñé's percolation structure.

N cells having identical area S_0 with given thickness t_{ox} (see Figure 2). It is assumed that gate oxide breakdown is triggered when critical number of defects (n_{bd}) occurs in at least one cell. Denote p_{bd} be the probability that any one cell breaks down, then the probability of gate oxide breakdown $F_{bd} = 1 - (1 - p_{bd})^N$. The probability to find a cell including k randomly distributed defects with average defect density $\bar{\lambda} = \bar{n}/S_0 t_{ox}$, where \bar{n} is the average number of defects per cell, is given by the Poisson distribution

$$p(k, \bar{\lambda}) = \frac{(\bar{\lambda} S_0 t_{ox})^k \exp(-\bar{\lambda} S_0 t_{ox})}{k!}, \quad k = 0, 1, 2, \dots \quad (4)$$

Because one cell breaks down when k reaches n_{bd} , the probability that a cell breaks down is

$$p_{bd}(\bar{\lambda}) = 1 - \sum_{k=0}^{n_{bd}-1} \frac{(\bar{\lambda} S_0 t_{ox})^k \exp(-\bar{\lambda} S_0 t_{ox})}{k!}, \quad (5)$$

and the probability of gate oxide breakdown is given by

$$F_{bd}(\bar{\lambda}) = 1 - \left\{ \sum_{k=0}^{n_{bd}-1} \frac{(\bar{\lambda} S_0 t_{ox})^k \exp(-\bar{\lambda} S_0 t_{ox})}{k!} \right\}^N, \quad (6)$$

for an MOSFET structure of area $S_T = NS_0$. This distribution function only depends on S_0 and n_{bd} , which are naturally related to the breakdown physics. For example, the distribution function of oxide breakdown is plotted at different cell areas and different critical number of defects in Figure 3, as the function of $\bar{\lambda}$. At this time, $t_{ox} = 4$ nm, and $N = 100$. Note that at identical $\bar{\lambda}$ and S_0 , the probability of oxide breakdown decreases as the critical number of defects increases. This percolation model, however, has the limitation to describe the dependence of n_{bd} on oxide thickness (see Stathis [15] for more details).

B. SPHERE-BASED PERCOLATION MODEL

Degraeve et al. [4] introduced a simulation-based percolation model dealing with the relation between oxide thickness and failure distribution, that is, “three-dimensional percolation model”. They considered a number of spherical defects randomly generated inside the oxide with fixed dimension. The only parameter of this model is a radius of the defect, r . If two neighboring spherical defects overlap, it is considered that conduction between these defects occurs. By modeling the interface as an infinite set of defects, the algorithm continuously generates spherical defects until a conducting path (called “percolation path”) is created from top to bottom of the oxide, and the oxide-breakdown event occurs

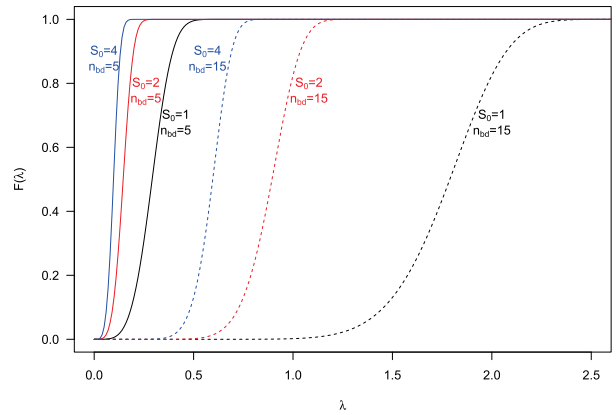


FIGURE 3. A distribution plot of oxide breakdown as the function of $\bar{\lambda}$.

(see Figure 1). The critical electron trap density can be calculated as the total number of generated traps divided by the volume of the oxide layer. The dimension of the oxide is chosen to be significantly larger than the sphere radius r , but sufficiently small enough to keep simulation time within a practical time frame. Through various simulations, they observed that the oxide breakdowns can be successfully modeled with the Weibull distribution and the Weibull shape parameter decreases as the oxide thickness decreases. Additionally their simulation results showed that if the oxide thickness gets smaller, the shape parameter of the Weibull distribution approaches to one, meaning that the failure distribution of ultrathin gate oxide becomes an exponential distribution (see Degraeve et al. [16] for details). However, their results are based mainly on randomly generated defects and do not consider clustered defects which have been often observed in the oxide layer.

C. CUBE-BASED PERCOLATION MODEL

Another percolation model assuming cubic defects was firstly suggested by Stathis [15]. Similar to Degraeve et al.'s approach [4], he defined oxide-breakdown as the formation of a percolation path. Instead, he used cubic defects on a fixed cubic lattice. The cubic defects are randomly generated on a cubic lattice of size $(l \times l \times m)$ according to a certain probability p_0 in the case of homogeneous percolation, or $p(s) = p_0 e^{-(s/\eta)}$ for gradient percolation. After placing all the defects under a given defect density distribution, the individual clusters are labeled in the lateral directions using a modified Hoshen-Kopelman algorithm [17] with periodic boundary conditions. All occupied sites at $(l \times l)$ face of the sample are assigned to the percolation cluster. The percolation model by Stathis [15] is based mainly on the Poisson statistics by assuming that defects are randomly generated in the oxide layer. It also successfully described the oxide breakdown with the Weibull distribution. This model, however, has a limitation in that only one defect can trigger oxide breakdown when the oxide thickness is smaller than cube size. Nevertheless, it has been widely adopted as an oxide breakdown model because the cubic lattice greatly

simplifies cluster identification along with significant reduction of computational time.

In summary, sphere- and cube-based percolation models are reasonable choices for simulating gate oxide failures than tile-based one. In a comparison of both models, the cube-based percolation model is a discretized approximation of the sphere-based approach for fast computation. The sphere-based model can reproduce more various defect patterns in a number of situations. Thus, it is recommended to adopt a sphere-based model if computing power is sufficient. However, its biggest drawback is that computational complexity increases exponentially with the number of defects generated during the simulation. Kim et al. [7] proposed a partitioned enumeration scheme for the sphere-based model in order to cope with the computation issue. It drastically reduced the computation burden by introducing the cube-based model concept where the oxide space is divided into cube cells.

IV. FRACTAL STRUCTURE FOR DEFECTS

As in the three percolation models, a Weibull distribution is an appropriate and widely accepted model for describing the time to the oxide breakdown. The Weibull distribution represents the “weakest” link characteristic of the breakdown process of gate oxides caused by generated defects [18]–[20]. The distribution function of a Weibull distribution is given by

$$F_T(t) = 1 - \exp[-(t/\alpha)^\beta], \quad (7)$$

where $\alpha (> 0)$ is a scale parameter and $\beta (> 0)$ is a shape parameter. The Weibull distribution can also be used to predict lifetime distribution of area-scaled gate oxides [21]. Consider two MOSFET devices with identical oxide thickness, but different area A_1 and A_2 , respectively. They have a breakdown distribution shifted with device area as

$$\frac{\alpha_1}{\alpha_2} = \left[\frac{A_2}{A_1} \right]^{1/\beta}, \quad (8)$$

where α_1 and α_2 are Weibull scale parameters having areas A_1 and A_2 , respectively, and β is a common shape parameter of the Weibull distribution. A smaller β means a greater sensitivity to the area. It is very important to accurately estimate the value of β because an incorrect estimation of β value results in a large error in extrapolated lifetimes of the oxides with different areas. Suñé et al. [14] recognized that general features of the breakdown distribution of thinner oxides can be accounted for by the area scaling model (8), where a critical defect density is needed to trigger a destructive breakdown. However, the area-scaling model (8) fails to represent actual real structure of defects in the gate oxide because it assumes that the gate oxide is divided by independent cells [21].

As an alternative, we introduce the fractal theory to describe breakdown statistics of area-scaled gate oxides as a complex system. Mandelbrot [22] introduced the word “fractal” to describe objects with the dimension smaller than the Euclidian dimensionality of underlying lattice or space. Nature provides numerous examples of fractal structures ranging from those with a fraction of the scale of the

universe down to those of atomic scale. These structures can be observed in the distribution of galaxies, cloud structures, mountain reliefs, turbulent flows on the surface of a planet like Jupiter, fractured rocks, rough surfaces, and disordered materials like percolation. Percolation plays a fundamental role in a considerable number of physical phenomena in which disorder is present within the medium [23]. Disordered media is composed of a random agglomeration of at least two types of materials. Examples include alloys, discontinuous deposits of metallic films, diluted magnetic materials, polymer gels, and general composite materials.

The fractal structure has two main properties: First, it satisfies the following power law relationship [23]

$$E[M(r)] \propto r^{d_f}, \quad d_f < d, \quad (9)$$

where $M(r)$ denotes a mass of the cluster with a radius r , d_f is the fractal dimension as a measure of how quickly the object moves away from the starting point, and d is the Euclidean dimension. Here, $E[\cdot]$ represents an expectation (or average). Because the average mass of the cluster is proportional to the number of quantities within a radius r , $E[N(r)]$, the equation (9) can be rewritten as

$$E[N(r)] = \kappa_0 \cdot r^{d_f}, \quad d_f < d, \quad (10)$$

for a constant κ_0 . Second, the fractal structure has self-similarity; an object with self-similarity is exactly or approximately similar to a part of itself. Mandelbrot [22] used a standard method for estimating the fractal dimension; that is, a large square lattice is divided into G^2 equal squares, and the number of squares intersected by the largest cluster is counted. Then, the fractal dimension d_f is determined through $N(r) \propto G^{d_f}$. A second method for estimating the fractal dimension is to take circles or spheres with increasing size, and to measure their contents or mass. Forrest and Witten [24] estimated the fractal dimension of two-dimensional electron microscope pictures of large smoke particles consisting of many small iron spheres of uniform size in this way.

The damage structures observed in dielectric breakdown have the form of trees in many cases. A tree is like a fractal or self-similar object in the sense that a branch of tree looks like a tree. Recently, Niemeyer et al. [25] showed that the simplest stochastic model of general dielectric breakdown leads to fractal structure. They introduced a stochastic model to simulate the growth of a fractal structure. Huo et al. [26] also used this fractal concept to analyze gate current noise phenomena in ultrathin gate oxide of pMOSFETs undergoing soft breakdown. Based on their results, we may regard percolation paths or spatial structures of defects in the oxide as statistical fractal structures. This assumption is extremely useful because the critical defect density of area-scaled gate oxide can be predicted based on the fractal dimension d_f without involving breakdown distributions of the oxides with different area.

Based on the fractal structure of spatial defects in oxides, we suggest a new approach for the breakdown of area-scaled oxides. If it is assumed that defects are randomly distributed

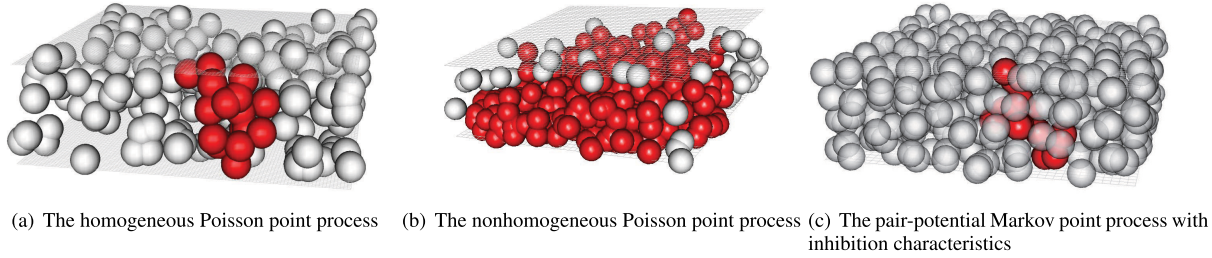


FIGURE 4. Simulated spherical defects with radius $r = 0.45$ nm at the oxide thickness $t_{ox} = 3$ nm and oxide area (20×20) nm² (a percolation path is represented by overlapped shaded-spheres).

in 3-dimensional space, that is, they follow a HPP with critical defect density λ_{bd} , then

$$\kappa_0 \cdot r^{d_f-3} \equiv \frac{E[M(r)]}{r^3} \propto \frac{E[N_{bd}(r)]}{l \times w \times t_{ox}} \equiv \lambda_{bd}, \quad (11)$$

for the oxide with length (l), width (w), and thickness (t_{ox}), from Eq. (9) and Eq. (10). Here, $N_{bd}(r)$ denotes critical number of defects in gate oxide with $(l \times w \times t_{ox})$ volume. Under assumption that the fractal dimension of defects in gate oxide depends on oxide thickness, the critical defect density for area-scaled oxide with thickness t_{ox} can be represented as

$$\lambda_{bd,t_{ox}} = \kappa_0 \cdot r^{d_f \cdot t_{ox} - 3}. \quad (12)$$

V. EXPERIMENTAL RESULTS

In context of percolation model, oxide breakdown occurs when a percolation path is created from the bottom to the top of the oxide layer. In order to investigate the impact of spatially distributed defects and oxide thickness dependence on the statistics of oxide breakdown, a variety of simulations are executed based on the percolation models. Because tile-based percolation model cannot explicitly represent thickness dependence on the oxide breakdown, sphere-based and cube-based percolation models are used in this experiment. The fractal structure of oxide breakdown according to oxide area is evaluated in terms of percolation conduction path via spatially generated defects.

A. RELATIONSHIP BETWEEN OXIDE THICKNESS AND DEFECT SIZE

First, we investigate the relationship between oxide thickness and critical number of defects (n_{bd}) for cube-shaped and sphere-shaped defects formed in random fashion. Spatial defects are generated from the HPP by assuming that the defects are uniformly distributed in the oxide layer. The defect radius r (edge length l) and oxide thickness t_{ox} are varied to investigate the characteristics of oxide breakdown distribution according to oxide thickness in the sphere-based (cube-based) percolation model. The simulations are repeated 100 times at same oxide thickness and defect size. The algorithm continues to generate defects until a conducting path is created from the top to the bottom of the oxide layer. Failure-time of the oxide is envisioned as the critical number of defects (n_{bd}) up to the creation of a percolation path connecting the two oxide interfaces by overlapped defects.

The simulated example of randomly generated spherical defects with radius $r = 0.45$ nm at oxide thickness $t_{ox} = 3$ nm and oxide area (20×20) nm² are given in Figure 4-(a). We confirmed that the Weibull distribution successfully fits all the failure-times of oxide layers with different thicknesses in sphere-based percolation model, as well as cube-based percolation model (even if the fitting results are not given here). For homogeneously generated spherical defects, it was observed that the values of Weibull shape parameter increase as the oxide thickness increases (see Table 1). Such trend was also observed in the simulation results by Degraeve et al. [21] for spherical defects. It is due to the fact that a smaller number of defects form the percolation path in thinner oxide and consequently there is a large statistical spread on the average density to form such a short path.

Next, we investigated thickness dependence on failure-times based on the spatial defects generated from the NHPP in the oxide. To generate the defects following the NHPP in the oxide layer, we applied the exponential decay model (1) in Khosru et al. [8]: $p(s) = k_0 e^{-s/\eta}$, $0 \leq s \leq t_{ox}$, where t_{ox} is the thickness of gate oxide. Since $\int_0^{t_{ox}} p(x)dx = 1$, the constant k is determined as $[\eta(1 - e^{-(t_{ox}/\eta)})]^{-1}$. In generating 3-dimensional defects in the oxide, we assumed a homogeneous spatial point process on planar region (x, y) and the exponential decay model (1) on z -axis. The plot of the simulated spherical defects, with size ($r = 0.45$ nm) at oxide thickness $t_{ox} = 3$ nm and oxide area (20×20) nm², are given in Figure 4-(b). At this time, the decay length from the interface was fixed at $\eta = 1.2$. We also simulated defects following the pair-potential Markov point process to examine localization effects of spatial defects in the oxide layer. The pair-potential function is selected to describe inhibition characteristics of defects in the oxide. The pair-potential function is: $\Psi_\theta(s) = -\log \gamma$ for $0 < s \leq \psi$, and 0 for $s > \psi$. It was noticed that the process was little different from the HPP when the parameter γ ranges $0.7 \sim 0.8$, hence γ was set at 0.6 in the consideration of computational time, and the Markov range ψ at $2 \times$ radius to make the percolation model be effective. The simulation plot of the spherical defects with size ($r = 0.45$ nm) is given in Figure 4-(c). We observed that the oxide breakdowns from defects following the NHPP and the pair-potential Markov point process can also be successfully fitted by the Weibull distribution. All of simulation results are given in Table 1.

TABLE 1. Simulation results for defects following several spatial point processes.

HPP with sphere defects					HPP with cubic defects								
t_{ox}	r	area	α	β	t_{ox}	l	area	α	β				
2	0.25	10 × 10	686.95	6.70	2	0.25	10 × 10	2929.59	10.11				
		20 × 20	2242.72	6.82			20 × 20	10493.89	11.00				
		40 × 40	6976.05	6.56			40 × 40	36709.17	10.42				
		0.45	10 × 10	98.18			3.24	0.5	10 × 10	286.53	4.44		
			20 × 20	258.19			3.60		20 × 20	858.56	5.38		
			40 × 40	665.24			3.69		40 × 40	2511.10	4.38		
	0.65	10 × 10	28.87	2.71		1	10 × 10	28.74	3.58				
		20 × 20	62.40	2.49			20 × 20	62.45	2.66				
		40 × 40	129.47	2.05			40 × 40	174.49	3.25				
	3	0.25	10 × 10	1282.32		10.03	3	0.25	10 × 10	5170.83	15.35		
			20 × 20	4378.09		8.84			20 × 20	18789.00	16.78		
			40 × 40	15069.90		11.17			40 × 40	70899.48	18.75		
		0.45	10 × 10	199.07		4.66		0.5	10 × 10	554.76	6.90		
			20 × 20	569.28		5.39			20 × 20	1901.49	8.14		
			40 × 40	1770.53		5.90			40 × 40	6238.64	8.36		
		0.65	10 × 10	60.83		3.36		1	10 × 10	59.49	3.79		
			20 × 20	169.49		4.03			20 × 20	149.61	3.63		
			40 × 40	435.69		3.93			40 × 40	420.61	3.59		
		6	0.25	10 × 10		3078.03		16.22	6	0.25	10 × 10	11683.72	33.26
				20 × 20		11366.50		17.83			20 × 20	44669.56	41.45
				40 × 40		42292.83		20.45			40 × 40	172075.09	38.60
	0.45		10 × 10	547.83		7.58	0.5	10 × 10		1415.17	16.47		
			20 × 20	1766.14		9.72		20 × 20		5208.38	18.12		
			40 × 40	6241.18		10.59		40 × 40		19040.95	16.87		
0.65	10 × 10		186.26	5.80	1	10 × 10	170.76	6.65					
	20 × 20		571.42	5.94		20 × 20	562.96	7.92					
	40 × 40		1815.06	7.44		40 × 40	1857.97	8.38					
NHPP with sphere defects					Pair-Potential Markov point process with inhibition								
t_{ox}	r		area	α	β	t_{ox}	r	area		α	β		
2	0.25		10 × 10	1296.74	4.25	2	0.25	10 × 10		940.03	9.75		
		20 × 20	4025.42	4.78	20 × 20			2976.56	6.12				
		40 × 40	11708.03	5.54	40 × 40			10369.47	9.19				
		0.45	10 × 10	108.45	2.85			0.45	10 × 10	135.81	3.21		
			20 × 20	352.68	2.90				20 × 20	344.22	4.01		
			40 × 40	819.76	3.24				40 × 40	981.08	4.70		
	0.65	10 × 10	11.68	2.29	0.65		10 × 10	33.16	2.00				
		20 × 20	88.67	2.14			20 × 20	80.72	3.11				
		40 × 40	191.77	2.17			40 × 40	154.38	2.61				
	3	0.25	10 × 10	4752.76	3.35		3	0.25	10 × 10	1630.78	8.75		
			20 × 20	13899.59	4.42				20 × 20	5920.82	11.28		
			40 × 40	41755.60	5.70				40 × 40	20903.93	23.76		
		0.45	10 × 10	379.45	2.40			0.45	10 × 10	271.32	5.89		
			20 × 20	1248.16	3.32				20 × 20	815.11	5.67		
			40 × 40	3345.77	5.25				40 × 40	2530.02	5.92		
		0.65	10 × 10	33.17	1.65			0.65	10 × 10	85.57	5.21		
			20 × 20	353.96	2.91				20 × 20	214.10	3.57		
			40 × 40	847.24	3.44				40 × 40	605.15	2.85		
		6	0.25	10 × 10	84464.94			4.48	6	0.25	10 × 10	4055.68	19.27
				20 × 20	208968			5.38			20 × 20	14846.66	28.86
				40 × 40	646477			6.75			40 × 40	54344.27	23.36
	0.45		10 × 10	6070.97	2.64		0.45	10 × 10		671.60	9.19		
			20 × 20	23306.36	3.30			20 × 20		2394.34	20.61		
			40 × 40	60715.37	3.52			40 × 40		8377.24	14.37		
0.65	10 × 10		589.70	1.73	0.65	10 × 10	225.81	6.3					
	20 × 20		5374.11	2.67		20 × 20	724.80	7.21					
	40 × 40		14411.88	3.58		40 × 40	2577.70	7.83					

In summary, failure density of the gate oxides decrease as oxide thickness decreases and defect size increases because relatively small number of defects can cause the oxide breakdown. The decreasing trend of Weibull shape parameter decrease with decreasing oxide thickness is also observed for breakdown distributions caused by defects following the NHPP and the pair-potential Markov point process with inhibition characteristic. It is also expected that decrease in oxide thickness will cause serious reliability concerns in both nonhomogeneous Poisson process and inhibition process.

B. AREA SCALING EFFECTS FOR OXIDE BREAKDOWN DISTRIBUTION

To investigate distributional characteristics of area-scaled gate oxides, we generated cube-shaped defects following the

HPP inside the oxide layer with the volume ($la \times wa \times ta$), where la , wa , and ta represent a length, a width, and a thickness of the gate oxide, respectively. Here, a lattice (cell) volume corresponds to a^3 . It is assumed that the length and the width are the same in this simulation; that is, $la = wa$. Because the cube-based percolation model has a structure to show area scaling effects on breakdown distribution more clearly than sphere-based percolation model, cubic defects with length $l = 0.5$ nm are used at this moment. The Weibull plot ($\log[-\log(1 - F)]$ vs. $\log(\text{defect density})$) for area scaled gate oxides, at different oxide thicknesses, are plotted in Figure 5. In general, the breakdown distribution for area-scaled gate oxides has been modeled by (8) along with the assumption about common shape parameter of a Weibull distribution. Simulation results show that the slopes (β) for

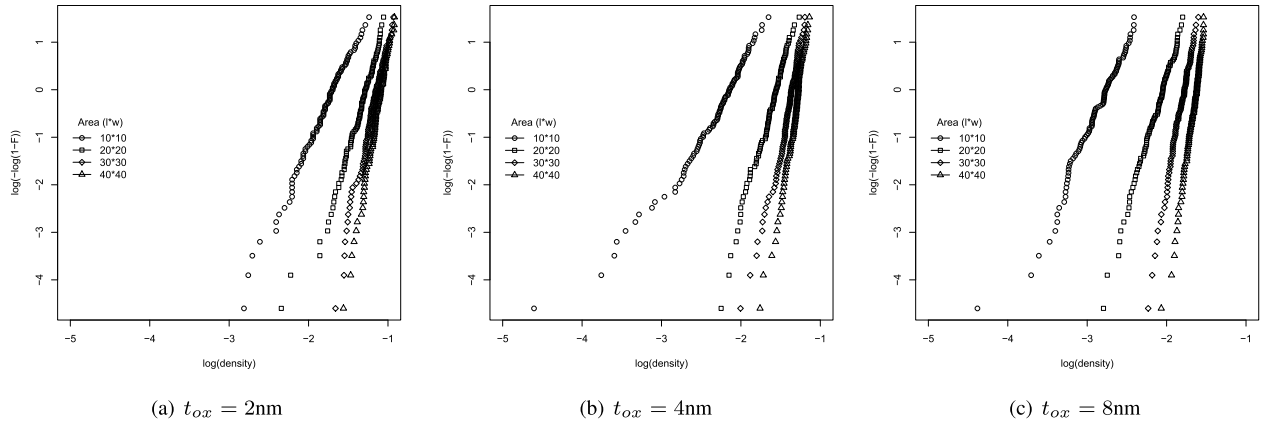


FIGURE 5. Weibull plot of critical defect densities for different oxide thicknesses along with various oxide areas.

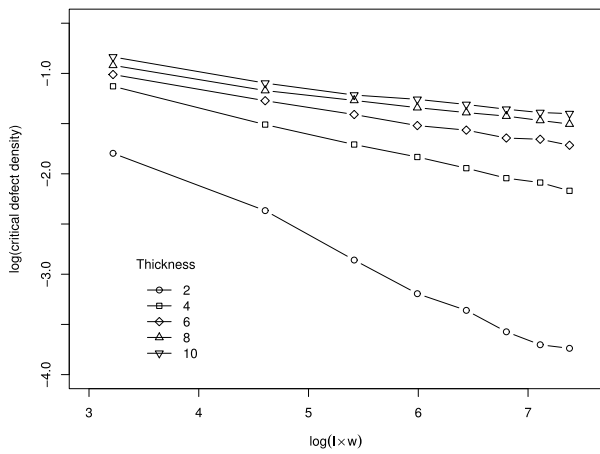


FIGURE 6. Log-transformed graph of critical defect density and oxide area.

gate oxides with different areas are not the same at same oxide thickness. It can be suspected whether there are confounding boundary effects in the simulations. However, even in simulation results at Table 1, we also observe that β for gate oxides with different areas are varied at same oxide thickness for any defects following both the HPP and the NHPP. Statistical tests for the same values of β for gate oxides at different areas rejected the null hypothesis $H_0 : \beta_i = \beta_j$ for $\forall i, j$. It means that large prediction error may exist when predicting area-scaled oxide reliability by assuming common shape parameters from equation (8) at identical oxide thickness.

We evaluated area-scaling effects through fractal structure of gate oxides with different areas, but same oxide thickness. First, we investigated the relationship between critical defect density and oxide area using Eq. (11). We performed 100 times Monte Carlo simulations for each oxide. Figure 6 shows log-log transformed graph of critical defect density and oxide area. The straight line indicates that defects in the gate oxide with same thickness have fractal structure with same fractal dimension $d_{f,t_{ox}}$ equivalent to the slope in the line. We estimated the fractal constant κ_0 and the fractal dimension by fitting the straight line using simple linear regression. Figure 7 shows the fractal dimensions for

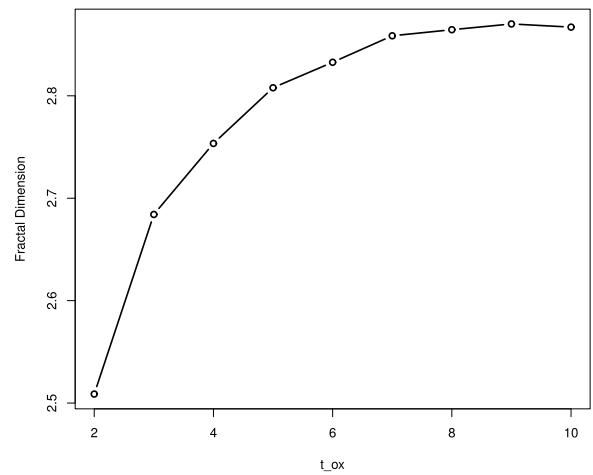


FIGURE 7. Fractal dimensions for each oxide thickness.

TABLE 2. Simulation results for area-scaled gate oxides based on the model (12).

t_{ox}	$d_{f,t_{ox}}$	κ_0	$A_2 (l \times w)$	$\hat{\lambda}_{bd,t_{ox}}$	$\lambda_{bd,t_{ox}}$
4	2.7535	0.7004	10 × 10	0.2251	0.2210
			20 × 20	0.1600	0.1600
			30 × 30	0.1310	0.1296
			40 × 40	0.1137	0.1143
8	2.8645	0.5971	10 × 10	0.3199	0.3102
			20 × 20	0.2651	0.2615
			30 × 30	0.2376	0.2405
			40 × 40	0.2197	0.2221

each oxide thickness. Based on the values, critical defect densities of gate oxides with different area A_2 are predicted by plugging the estimates in (12), where $r \equiv l \equiv w$. The results are summarized in Table 2 for true defect densities ($\lambda_{bd,t_{ox}}$) calculated from data sets. Note that the biases are negligible. The critical defect density of area-scaled gate oxides can be predicted by only examining fractal structure through the fractal dimension $d_{f,t_{ox}}$ without involving breakdown distributions of the oxides with different areas.

VI. CONCLUSION

Continuous size reduction of MOSFET devices for increasing circuit speed and improving packing density are expected to

cause serious reliability concerns to semiconductor manufacturers. To accurately predict reliability of newly developed MOSFET devices with ultra-thin gate oxide, spatial patterns of defects generated inside the oxide, as well as defect generation mechanisms, must be explicitly reflected in reliability model.

We discussed several percolation models by envisioning oxide failure as creation of a percolation path connecting two oxide interfaces by overlapped defects. Because the percolation model depends highly on the patterns of defect generation, the defect patterns following popular spatial point processes are investigated based on physical defect generation models. It was observed that the Weibull distribution successfully fits the breakdown data caused by creation of a percolation path connecting two oxide interfaces. However, simulation results showed that the shape parameter in the Weibull distribution depends on oxide area, hence existing area-scaling model may provide biased prediction results by assuming common shape parameter regardless of oxide areas. As an alternative, we proposed a new method to evaluate lifetimes of area-scaled gate oxides of MOSFET devices mainly through their fractal structure. We observed that defects in gate oxide can be modeled via fractal structure, and they have same fractal structure at identical oxide thickness.

In recent years, high-k gate stack structure is widely adopted to reduce leakage current problems caused by tunnelling [28]. Therefore, time dependent dielectric breakdowns with high-k materials are expected to be a prominent study to more accurately project lifetimes of the MOSFET devices [29]. In this regard, further understanding for physical models of gate stacks with high-k materials is required to accurately project the failures of MOSFET devices in future research.

APPENDIX A SPATIAL HOMOGENEOUS POISSON PROCESS

Consider a point process $\{\mathcal{N}(A) : |A| \geq 0\}$ on any disjoint sequence of d -dimensional planar regions $A \in \mathfrak{R}^d$, where $\mathcal{N}(A)$ is the number of events on A and $|A|$ is the area of A . A point process $\mathcal{N}(\cdot)$ is defined as a homogeneous Poisson process with intensity $\lambda (> 0)$ when the number of events in any bounded region A has a Poisson distribution with mean $\lambda|A|$, that is, for independent random variables $\mathcal{N}(A)$,

$$p_k \equiv Pr(\mathcal{N}(A) = k) = e^{-\lambda|A|} \frac{(\lambda|A|)^k}{k!}, \quad k = 0, 1, 2, \dots$$

Let $\mathbf{x}_1, \dots, \mathbf{x}_n$ be the locations of n traps. In the HPP, given $\mathcal{N}(A) = n$, $\mathbf{x}_1, \dots, \mathbf{x}_n$ are independently and identically distributed uniformly on A partitioned by A_1, \dots, A_n , i.e.

$$\begin{aligned} Pr(\mathbf{x}_1 \in A_1, \dots, \mathbf{x}_n \in A_n) \\ &= Pr(\mathbf{x}_1 \in A_1) \times \dots \times Pr(\mathbf{x}_n \in A_n) \\ &= \frac{|A_1|}{|A|} \times \dots \times \frac{|A_n|}{|A|}. \end{aligned}$$

Uniformity refers to the fact that the traps exhibit no tendency to occupy particular regions of the space, while independence

suggests that the location of a given trap is determined without reference to that of any other trap.

APPENDIX B SPATIAL NONHOMOGENEOUS POISSON PROCESS

A NHPP $\mathcal{N}(A)$ is defined on a finite planar region A with the following postulates:

- (i) The number of events in any bounded region A , $\mathcal{N}(A)$ has a Poisson distribution with mean $\Lambda(A) = \int_A \lambda(\mathbf{x}) d\mathbf{x}$, for $\mathbf{x} \in A$, where $\lambda(\mathbf{x})$ is the intensity function on A defined as

$$\lambda(\mathbf{x}) \equiv \lim_{|d\mathbf{x}| \rightarrow 0} \frac{E[\mathcal{N}(d\mathbf{x})]}{|d\mathbf{x}|},$$

where $E[\cdot]$ denotes an expectation (or average).

- (ii) Given $\mathcal{N}(A) = n$, the n events form an independent sample from the distribution on A with a probability density function proportional to $\lambda(\mathbf{x})$.

This general framework on the NHPP can be used to define systems on a finite region \mathfrak{R} by choosing the intensity function to restrict λ to \mathfrak{R} , that is; $\lambda_{\mathfrak{R}}(\mathbf{x}) = \lambda(\mathbf{x})$ for $\mathbf{x} \in \mathfrak{R}$, and 0, otherwise. The nano-structure functions for such finite systems (i.e., oxide layer with finite region) are then calculated by using $\lambda_{\mathfrak{R}}$ in place of λ . Constructing realizations of the NHPP can be easily done in two stages if the density function $\lambda(\mathbf{x})$ is bounded on \mathfrak{R} , say, $\lambda(\mathbf{x}) \leq \lambda^*$. First, a Poisson process of density λ^* is simulated. Second, the resulting point pattern is thinned. Each point \mathbf{x} , independently of the other points, is kept with probability $\lambda(\mathbf{x})/\lambda^*$ or deleted with probability $1 - \lambda(\mathbf{x})/\lambda^*$. The resulting point pattern is reduced to a NHPP with intensity function $\lambda(\mathbf{x})$. Finally, we place spheres of common radius r on the points of $\mathcal{N}(\cdot)$ to construct a realization of inhomogeneously Poisson distributed traps.

APPENDIX C PAIR-POTENTIAL MARKOV POINT PROCESS

The pair-potential Markov point process is expressed in terms of a pair-potential function $\{\Psi_{\theta}(s) : \theta \in \Theta\}$, indexed by a parameter vector θ in a parameter space Θ for Euclidian distance s . An observed spatial point process in some area A is Markov of range ψ if the conditional intensity at point \mathbf{x} , depends only on the events in the circle of radius ψ centered at \mathbf{x} .

Define a function of the distance between traps x_i and x_j as

$$h(x_i, x_j) = -\Psi(\|x_i - x_j\|), \quad x_i \neq x_j,$$

and two events interact are called neighbors if their distance $\|x_i - x_j\|$ is less than ψ . At the start, we assume that there are no large-scale effects ($h(x_i, x_j) \equiv 0$) and no higher-order interactions. Then, the number of traps and the ordered n -tuple of their locations are jointly distributed according to the Gibbs grand canonical distribution [27] as

$$f((x_1, \dots, x_n), n) = \frac{e^{-v(A)}}{\alpha n!} \exp \left\{ - \sum_{1 \leq i < j \leq n} \Psi(\|x_i - x_j\|) \right\},$$

